12 May 2000

ELSEVIER

Chemical Physics Letters 322 (2000) 111–118

CHEMICAL PHYSICS LETTERS

www.elsevier.nl/locate/cplett

Noise triggering of radiation damping from the inverted state

Matthew P. Augustine [a,*], Seth D. Bush [b], Erwin L. Hahn [b]

[a] *Department of Chemistry, One Shields Avenue, University of California, Davis, CA 95616, USA*
[b] *Departments of Chemistry and Physics, University of California, Berkeley, CA 94720, USA*

Received 14 March 2000; in final form 23 March 2000

Abstract

Spontaneous radiation damping in nuclear magnetic resonance spectroscopy of sharp lines is commonly encountered in highly magnetized samples following magnetization inversion. The time delay for the maximum of the hyperbolic secant like signal to develop following inversion is measured and calculated. The distribution function of the measured delay times is Gaussian–Boltzmann and can be used to predict the sensitivity of both signal delay and phase to inversion errors.

An inverted two-level system coupled to a cavity at resonance emits coherent radiation spontaneously above or at the maser threshold condition. This applies to nuclear magnetic resonance (NMR) as a special case [1] of radiation damping [2] for the condition $T_2/T_R \geqslant 1$. The inverse line width is given by T_2, and the radiation damping time T_R, is defined by

$$T_R = (2\pi\gamma M_0 Q\xi)^{-1} \tag{1}$$

where M_0 is the equilibrium magnetization, γ is the gyromagnetic ratio, Q is the cavity figure of merit, and ξ is the sample filling factor. In general, a θ_0 pulse applied to the entire spin ensemble is followed by completion of a radiation damping signal, and the magnetization ends up along the polarizing field with a lesser final energy, having dissipated energy into the circuit resistance [1] [3,4]. From the initial θ_0 orientation, the total angle $\Delta\theta$ through which the magnetization component at exact resonance tilts toward the ground state is given by [5]

$$|\Delta\theta| = \frac{T_2}{T_R}\sin(\theta_0 - |\Delta\theta|). \tag{2}$$

Here T_2 is determined by symmetric inhomogeneous broadening. For an exact $\theta_0 = \pi$ inversion pulse, the transcendental Eq. (2) reduces to

$$|\Delta\theta| = \frac{T_2}{T_R}\sin|\Delta\theta|. \tag{3}$$

Eq. (3) specifies that the spin system may end up in either of two final states, as indicated in Fig. 1. For $|\Delta\theta| \neq 0$, emission of radiation must occur, leading toward a final lower energy polarization state; or for

* Corresponding author. Fax: +1-530-752-8995; e-mail: augustin@chem.ucdavis.edu

[1] Analogous to coherent optical superradiant emission appearing in the form of propagation.

0009-2614/00/$ - see front matter
PII: S0009-2614(00)00390-0

$|\Delta\theta| = 0$, the exactly inverted polarization remains in a metastable inverted state and does not radiate even if the condition $T_2/T_R \geqslant 1$ applies. The latter condition of trapping in the inverted state must always occur first if the magnetization has been prepared in an exact inverted state because there is no radiating polarization that can couple to the tuned circuit. After a time delay [6,7] the two-level system will escape from the metastable state and radiate coherently if a weak perturbation of some kind tilts the magnetization sufficiently away from its initial exact π alignment. Room temperature rf noise is the ever present perturbation of importance. After the circuit noise field H_{1n} initiates a small tilt angle away from the $-z$ direction defined by θ_-, the radiation damping reaction field H_{1R} comes into play and reinforces the increase in θ_-. As θ_- increases at random, both the mean square angle $\langle \theta_-^2 \rangle$ and the H_{1R} reaction field increase along with it. It will be seen that the combined effects of H_{1n} and H_{1R} lead to the development of amplified spin noise in the inverted state and to the establishment of steady state spin noise [8] in the equilibrium ground state. The solid lines in Fig. 2 define both the transverse in-phase u and quadrature out-of-phase v components of the signal following a π rf pulse. The dashed line corresponds to the envelope of the signal. The time t_0 is measured from the π rf pulse to the maximum of this signal. The time t_{delay} corresponds to the average value for t_0 following many measurements of signals like those in Fig. 2. The signal phase at t_0 can also be extracted from these signals as $\arctan(v/u)$ as shown in Fig. 2.

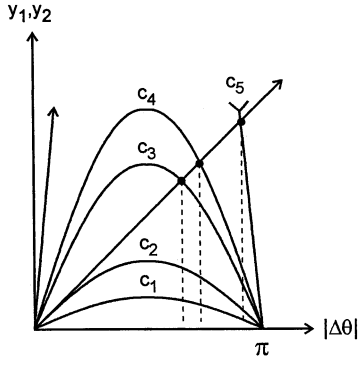

Fig. 1. Graphical solutions to the transcendental Eq. (3) as a function of $c_n = T_2/T_R$. In all cases the metastable inverted state $|\Delta\theta| = 0$ is a solution. However, when $c_n > 1$, $|\Delta\theta| \neq 0$ values exist. Under these conditions, circuit noise stimulates the transition to the ground state.

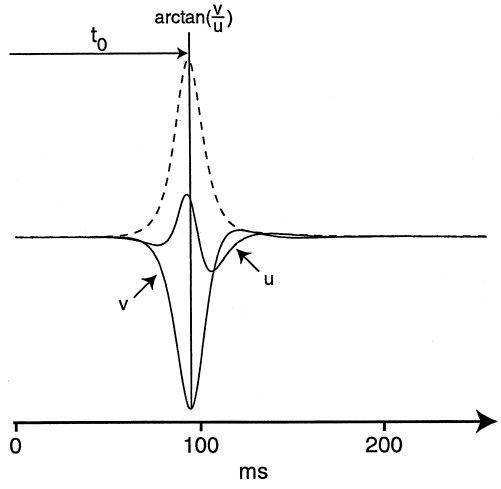

Fig. 2. An example of the signal measured following a π rf pulse applied to a H_2O/D_2O (95:5%) solution at a 600 MHz ^1H Larmor frequency for $T_R = 7.1$ ms. The two solid lines correspond to the in-phase u and out-of-phase v magnetization, while the dashed line labels the signal envelope. The time from completion of the rf pulse to the signal maximum defines t_0 as shown by the arrow in the figure. For a given T_R, circuit noise will vary the time t_0 and the phase of the signal $\arctan(v/u)$ at t_0 from experiment to experiment. Therefore, the time t_{delay} calculated here is the most probable value of t_0 extracted from many measurements.

To evaluate the time t_{delay} and to introduce some nomenclature, consider first the equation for the tilt angle θ of the magnetization from the $+z$ direction in the sharp line limit $T_2 = \infty$:

$$\frac{d\theta}{dt} = -\frac{\sin\theta}{T_R}. \tag{4}$$

The hyperbolic secant solution [2] to this equation is proportional to the transverse magnetization

$$v = M_0 \sin\theta = M_0 \operatorname{sech}\left(\frac{t - t_0}{T_R}\right) \tag{5}$$

where

$$t_0 = T_R \operatorname{arcsech}(\sin\theta_0) = T_R \ln\left(\frac{2}{\tan\theta_0}\right) \tag{6}$$

defines the duration of signal coherence extending from the application of any θ_0 pulse at $t=0$ to the maximum of the signal given by Eq. (5) at $t=t_0$. Any fluctuations in the direction of the magnetization due to an incoherent circuit noise field H_{1n} introduces an additional term $\dot{\theta}_n=\gamma H_{1n}$ into Eq. (4). A Langevin equation of the form

$$\frac{\mathrm{d}\theta}{\mathrm{d}t}+\frac{\theta}{T_R}=\dot{\theta}_n \tag{7}$$

is obtained in the small tip angle limit $\sin\theta\approx\theta$ near the ground state. We first apply Eq. (7) to evaluate the approach to thermal equilibrium when a balance in the ground state is reached between the emission of radiation damping and the circuit noise field stimulated absorption [8]. (Following this analysis, Eq. (7) will then be modified to deal with non-equilibrium time delay effects after inversion of the magnetization when the circuit noise field induces stimulated emission instead of absorption.) The time dependence of the average of the mean square deviation of the magnetization from the $+z$ direction, given by

$$\frac{\mathrm{d}\langle\theta^2\rangle}{\mathrm{d}t}+\frac{2\langle\theta^2\rangle}{T_R}=2\langle\theta\dot{\theta}_n\rangle \tag{8}$$

is obtained from Eq. (7) in the usual way by using the identity $\mathrm{d}\theta^2/\mathrm{d}t=2\theta\,\mathrm{d}\theta/\mathrm{d}t$ followed by application of an ensemble average as denoted by the paired brackets. To determine $\langle\theta\dot{\theta}_n\rangle$, consider Eq. (8) at steady state equilibrium where $\langle\theta^2\rangle=\langle\theta\dot{\theta}_n\rangle T_R\ll 1$. The equipartition theorem for the energy excess in the θ degree of freedom is given by

$$\langle\vec{M}\cdot\vec{H}\rangle-M_0H_0=M_0H_0(\langle\cos\theta\rangle-1)$$
$$\approx\frac{M_0H_0}{2}\langle\theta^2\rangle=kT_c/V_s \tag{9}$$

where k is Boltzmann's constant, H_0 is the magnetic field, V_s is the sample volume, and T_c is the temperature of the circuit resistance. Eq. (9) is then applied to Eq. (8) to evaluate the quantity $\langle\theta\dot{\theta}_n\rangle$, and the solution for $\langle\theta^2\rangle$ becomes

$$\langle\theta^2\rangle=\frac{2kT_c}{M_0H_0V_s}\left[1-\exp(-2t/T_R)\right]. \tag{10}$$

At $t=\infty$ this equation indicates that on average the single magnetization vector initially aligned along the $+z$ direction will spread to a final mean square angular width $\langle\theta^2\rangle_\infty$ due to the balance between absorption caused by H_{1n} and emission caused by H_{1R}. This mean square angle established at equilibrium for $I=1/2$ is given by

$$\langle\theta^2\rangle_\infty=\frac{2kT_c}{M_0H_0V_s}=\frac{\langle M_x^2\rangle+\langle M_y^2\rangle}{M_0^2}=\frac{N\gamma^2\hbar^2}{2M_0^2}, \tag{11}$$

identical to that anticipated for spin noise fluctuations [8] when the temperature T_c is equal to the lattice temperature T_{lat}. In the more general case when $T_c\neq T_{lat}$, the right-hand side of Eq. (11) must be multiplied by T_c/T_{lat}.

More explicitly, it follows that $\langle\theta^2\rangle_\infty=\gamma^2\langle H_{1R}^2\rangle T_R^2=\gamma^2\langle H_{1n}^2\rangle T_R Q/\omega$ defines the thermal equilibrium angle where $\langle H_{1R}^2\rangle=\langle H_{1n}^2\rangle Q/T_R\omega$ and $\langle H_{1n}^2\rangle=4\pi kT_c/V_c$ is obtained from the Nyquist theorem. Thus the average intensity of the radiation damping field emission is balanced by the fraction $Q/T_R\omega$ of the circuit noise field intensity of absorption within the bandwidth $1/T_R$ of the spins, neglecting relaxation. Data obtained at 600 MHz gives $\langle\theta^2\rangle_\infty=7\times10^{-14}\ rad^2$ and $T_R=10$ ms, yielding $\langle H_{1R}^2\rangle^{1/2}\approx 1$ nG.

Before proceeding with the calculation of t_{delay}, one must be completely aware of the experimental conditions. To achieve essentially exact initial alignment in practice, care must be taken to avoid a small initial tilt angle of the inverted magnetization due to slight inaccuracies in pulse width, the inhomogeneity of the applied rf field over the sample, and excitation caused by insufficiently shielded rf leakage. This leakage is avoided by using both high isolation rf switches and incorporating additional crossed diodes between the rf-transmitter and NMR probehead. Unwanted macroscopic coherence due to pulse width errors and rf inhomogeneity are removed by the application of a sufficiently strong DC field gradient pulse just after the π rf pulse. Care must be exercised in the choice of field gradient pulse shapes. The eddy currents due to square pulses tend to produce transients that reintroduce small tipping of the inverted magnetization. These effects were mini-

mized in all measurements by using a 10 ms Gaussian gradient pulse shape having a 29 G/cm peak amplitude and 4 ms full width at half height. While radiation damping dominates the evolution with a line width of 10 Hz, during the 10 ms gradient pulse period the linewidth jumps from ≈ 10 Hz to ≈ 250 kHz and radiation damping is suppressed. This can be justified from Eq. (3) by comparing $|\Delta\theta|$ for both the 10 Hz and 250 kHz wide lines where $T_2 = 100$ and 4 ms, respectively. Taking $T_R = 5$ ms gives $|\Delta\theta| = 0°$ and 171.4° for the narrow line, indicating that both the metastable and ground state are accessible to the magnetization as shown in Fig. 1 for c_3, c_4, and c_5. On the other hand, for the same T_R value, the wide line gives only $|\Delta\theta| = 0$, suggesting that radiation damping does not effect a rotation of the magnetization towards the ground $+z$ direction as shown in Fig. 1 for c_1 and c_2. Since application of the gradient has the dual effect of removing any unwanted tilt and suspending the effects of radiation damping, the development of $\langle \theta_-^2 \rangle$ from zero due to nearly exact alignment along the $-z$ direction immediately after the field gradient pulse can be evaluated.

The solution for the time delay

$$t_0 = T_R \ln\left(\frac{2}{\theta_-}\right) \tag{12}$$

may be expressed in terms of the small tip angle θ_- from the $-z$ direction using Eq. (6), where $\theta_0 = \pi - \theta_-$ and $\tan\theta_- \approx \theta_-$. In the inverted state, M_0 changes sign and the sign of T_R changes in Eq. (10) to give

$$\langle \theta_-^2 \rangle = \langle \theta^2 \rangle_\infty \left[\exp(2t/T_R) - 1\right]$$

$$= \theta_-^2 = 4\exp\left[2(t - t_0)/T_R\right] \tag{13}$$

after equating Eq. (10) to Eq. (5) in the small angle limit. Eq. (13) exhibits gain in the exponential regime of Eq. (6) but can only be applied for restricted times $0 < t < t_{delay}$. Therefore $\langle \theta_-^2 \rangle$ may be equated with the solution for θ_-^2 from Eq. (5) in the exponential regime near $t = 0$, but where $t = t'$ is large enough so that in Eq. (13)

$$\langle \theta_-^2 \rangle \approx \langle \theta^2 \rangle_\infty \exp\left[2t'/T_R\right] \gg \langle \theta^2 \rangle_\infty . \tag{14}$$

Therefore a connection is made between the incoherent and coherent properties of the tipping magnetization for $\theta_- \ll 1$. The time t' is chosen long enough so that the coherence of angle $\gamma H_{1R} T_R$ associated with H_{1R} dominates over the smaller induced incoherent angle caused by H_{1n} field fluctuations from the circuit. Under these conditions, the solution for t_0 in Eq. (14) leads directly to the average time

$$t_{delay} = \frac{T_R}{2} \ln\left(\frac{4}{\langle \theta^2 \rangle_\infty}\right). \tag{15}$$

The paradox that $t_0 = \infty$ obtained from Eq. (12) when $\theta_- = 0$ is thus avoided when M_0 is perfectly inverted after an ideal π pulse. Instead, after sufficient time t' the diffusion Eq. (13) develops an intermediate mean square angle $\langle \theta_-^2(t') \rangle$ which defines

$$t' = \frac{T_R}{2} \ln\left(\frac{\langle \theta_-(t')^2 \rangle}{\langle \theta^2 \rangle_\infty}\right). \tag{16}$$

This means that $\langle \theta_-(t')^2 \rangle = \gamma^2 H_{1R}^2 T_R^2 \gg \langle \theta^2 \rangle_\infty$ specifies a coherent tipping angle much larger than any tipping caused by $\langle H_{1n}^2 \rangle$ due to circuit noise. The coherent relation Eq. (12) then gives an additional delay time

$$t_0' = \frac{T_R}{2} \ln\left(\frac{4}{\langle \theta_-(t')^2 \rangle}\right) \tag{17}$$

to be added to t'. The sum $t_0' + t' = t_{delay}$ is again given by Eq. (15). The essential assumption here is that while incoherence is dominant, the relation Eq. (15) which is obtained for a coherent model cannot be applied. It is only valid when initial angles θ_- in the distribution are large enough above the influence of circuit noise so that they appear equivalent to coherent initial tip angles θ_0 in Eqs. (2) and (6). The sum of the logarithms given by $t_0' + t'$ reduces to a t_{delay} independent of t itself because $\langle \theta_-(t')^2 \rangle$ cancels out leaving only the dependence on the equilibrium mean square angle $\langle \theta^2 \rangle_\infty$.

From knowledge of the mean square thermal equilibrium angle $\langle \theta^2 \rangle_\infty$ a Boltzmann probability distribution in θ_- may defined as

$$P(\theta_-) = \frac{1}{\sqrt{2\pi\langle \theta^2 \rangle_\infty}} \exp\left[-\theta_-^2/\left(2\langle \theta^2 \rangle_\infty\right)\right] \tag{18}$$

that can be applied immediately following application of the field gradient pulse. The probability that M_0 is oriented at any initial angle θ_- is determined by the distribution $P(\theta_-)$. The average value of the time delay is then given by the normalized average

$$t_{\text{delay}} = \langle t_0 \rangle = T_R \sqrt{\frac{2\pi}{\langle \theta^2 \rangle_\infty}} \times \int_0^\pi \ln\left(\frac{2}{\theta_-}\right) P(\theta_-) \sin\theta_- \, d\theta_- . \qquad (19)$$

This expression incorporates the solid angle weighting factor $(\sin\theta_-/2)$ of M_0 on the unit sphere about the $-z$ direction. Note that the application of $\sin\theta_-$ in Eq. (19) implies that for $\theta_- = 0$ the single vector magnetization is never exactly aligned along the z axis. It is in fact tipped slightly off axis in a direction representing an eigenstate of the magnetization because the spin system is coupled to the single mode of the cavity [8] as well as to the field H_0. It turns out that t_{delay} expressed by Eq. (15) depends upon the most probable (peak) value $\theta_-^2 = \langle \theta^2 \rangle_\infty$ of the weighted distribution $\sin\theta_- P(\theta_-) \approx \theta_- P(\theta_-)$ in Eq. (19), at which t_0 displays its average value.

The validity of the expressions for t_{delay} in Eqs. (15) and (19) for the probability were tested experimentally using the ^{1}H signal in H_2O/D_2O mixtures at 600 MHz as shown in Fig. 3. For a specific T_R value the histograms summarize 250 separate measurements of t_0. A summary of experimental T_R, $\langle \theta^2 \rangle_\infty$, and t_{delay} values measured from the width and center of the hyperbolic secant bursts summarized in Fig. 3 is provided in Table 1 along with a comparison to theoretical estimates of these parameters from Eqs. (1), (11) and (15) with $Q\xi = 9.3$. Superimposed on each histogram for each choice of T_R in Fig. 3 is a solid line representing the distribution of t_0 determined from the T_R value calculated from Eq. (1) and the $\langle \theta^2 \rangle_\infty$ value calculated from Eq. (15) and t_{delay}. Here the abscissa is determined from Eq. (15) by scaling $\langle \theta^2 \rangle_\infty^{1/2}$ from its peak value by an amount $\pm\delta\theta_-$, while the ordinate is calculated from Eq. (18) using $\theta_- = \langle \theta^2 \rangle_\infty^{1/2} \pm \delta\theta_-$. Returning to Table 1, both the experimental and theoretical T_R and t_{delay} values are consistent for the three highest concentrations. The shape of the curve

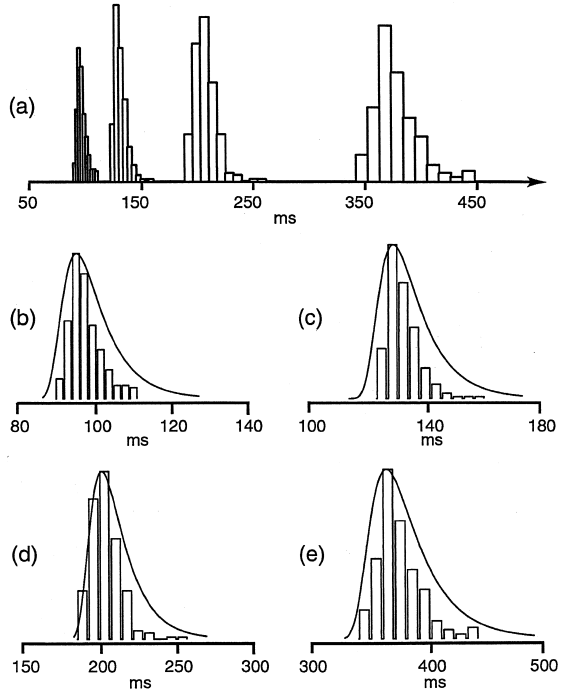

Fig. 3. Summary of t_0 measurements for H_2O/D_2O (95:5%), H_2O/D_2O (75:25%), H_2O/D_2O (50:50%), and H_2O/D_2O (25:75%) solutions in (b), (c), (d), and (e), respectively. Each histogram represents 250 separate determinations of t_0 at each concentration or equivalently each specific T_R. The time t_{delay} at each T_R corresponds to the average value of the distribution in Eq. (18) as seen in the compilation in (a). These values for t_{delay} along with theoretical estimates are provided in Table 1. The solid line in each graph corresponds to the distribution anticipated from Eq. (18).

predicted by Eq. (19) is similar to that predicted by Glauber [9]. The NMR measurements in Fig. 3 more literally conform to the theoretical predictions of Eq. (19) than do previous optical measurements by Vehren [10] in an inhomogeneously broadened optical two-level system with damping [11].

One source of error between experimental and theoretical $\langle \theta^2 \rangle_\infty$ values could lie in the assumption that the gradient pulse completely removes any initial tip angle, and therefore the Gaussian distribution $P(\theta_-, \phi_-)$ in the angle θ_- becomes skewed. For perfect inversion, the distribution in signal phase ϕ_- is expected to be random since $P(\theta_-)$ is independent of ϕ_-. Fig. 4 summarizes the distribution of phases at t_0 extracted from the same 250 measurements used to determine t_{delay} in Fig. 3. Fig. 4a represent-

Table 1
Summary of theoretical and experimental values

H_2O (%)	t_R		$\langle\theta^2\rangle_\infty$		T_{delay}	
	Experiment (ms)	Theory (ms)	Experiment	Theory	Experiment (ms)	Theory (ms)
95	7.1	7.0	1.2×10^{-11}	7.0×10^{-14}	96.6	110.8
75	9.8	9.0	1.1×10^{-11}	9.8×10^{-14}	131.4	141.0
50	15.0	13.3	7.9×10^{-12}	1.5×10^{-13}	207.3	205.6
25	27.6	26.6	1.0×10^{-11}	3.0×10^{-13}	377.7	401.9

ing the highest H_2O concentration is clearly a random phase distribution while the data for both the 75% and 25% H_2O concentrations in Fig. 4b,d deviate from the completely random result. Most pronounced is the very tight distribution about 89° for the data in Fig. 4c. The data in Fig. 3a, Fig. 4a, and Table 1 indicate that the discrepancy between experimental and theoretical $\langle\theta^2\rangle_\infty$ values persists even when inversion performance is nearly ideal. A likely cause of this error is linebroadening due to magnetic field inhomogeneity, an effect not included in the current treatment. To account for the phase deviations for the three other ^1H concentrations studied here, the distribution in Eq. (18) must be adjusted to account for a small tip angle η remaining after application of the field gradient pulse. Here, the distribution is still independent of phase χ about the axis tipped away from the $-z$ direction by the angle η, but dependent on both polar angles θ_- and ϕ_- concentrated on the $-z$ axis. Recasting the distribution in terms of the θ_- and ϕ_- polar angles as in shown in Fig. 5 gives

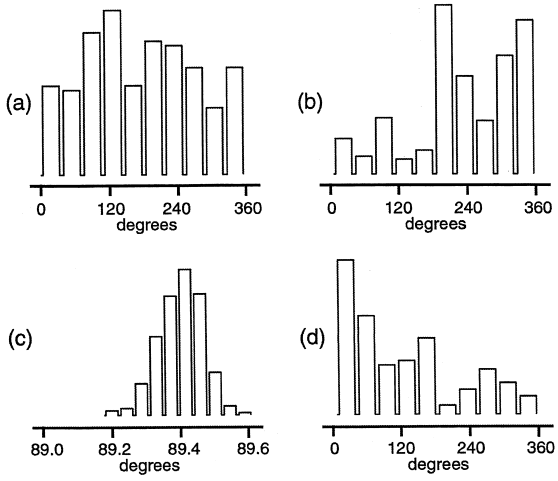

Fig. 4. Summary of signal phase measurements at $t=t_0$ for H_2O/D_2O (95:5%), H_2O/D_2O (75:25%), H_2O/D_2O (50:50%), and H_2O/D_2O (25:75%) solutions in (a), (b), (c), and (d), respectively. Each histogram represents 250 separate determinations of the phase at each T_R value. The phase in (a) is random as expected from the distribution in Eq. (18) but the spread of the data in (b), (c), and (d) display a phase buildup at 220°, 89°, and 0°, respectively. The departure from random phase and its anisotropy caused by small tip angle η in (c) is explained with the distribution function in Eq. (20) and does not generate appreciable error in the time t_{delay}.

$$P(\theta_-,\phi_-)=\frac{1}{\sqrt{2\pi\langle\theta^2\rangle_\infty}}\exp\Big[-\big(\eta^2+\theta_-^2-2\eta\theta_-\cos\phi_-\big)/\big(2\langle\theta^2\rangle_\infty\big)\Big] \qquad (20)$$

which can be used to determine just the distribution in ϕ_- by weighting $P(\theta_-,\phi_-)$ by θ_-, normalizing, and integrating over the variable θ_-:

$$P(\phi_-)=\sqrt{\frac{2\pi}{\langle\theta^2\rangle_\infty}}\int_{-\infty}^{+\infty}P(\theta_-,\phi_-)\theta_-\,\mathrm{d}\theta_-$$
$$=\exp\Big[-\big(\eta^2\sin^2\phi_-\big)/\big(2\langle\theta^2\rangle_\infty\big)\Big]\times\left(1+\eta\cos\phi_-\sqrt{\frac{2\pi}{\langle\theta^2\rangle_\infty}}\right). \qquad (21)$$

For $\eta=0$ the distribution centered around the $-z$ direction is uniform from $0\leqslant\phi_-\leqslant2\pi$. As η is

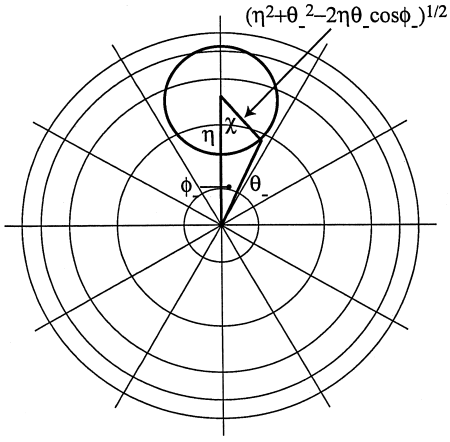

Fig. 5. Graphical determination of the Gaussian probability distribution appropriate for tip angle error. The Gaussian is symmetric in the angle χ about the axis inclined by angle η away from the $-z$ direction. The displacement in terms of η, θ_-, and ϕ_- for small θ_- can be determined by the law of cosines.

increased, the distribution of phase begins to concentrate around the direction of η. As the term proportional to $\eta\cos\phi_-$ in Eq. (21) becomes negative for $\pi/2 \leqslant \phi_- \leqslant 3\pi/2$ values and less than -1, $P(\phi_-)$ becomes a negative probability and the values of ϕ_- that satisfy this condition cannot occur. Very large values of η cause the phase distribution in the regions from $0 \leqslant \phi_- \leqslant \pi/2$ and $3\pi/2 \leqslant \phi_- \leqslant 2\pi$ to concentrate in a narrow region along the direction of η as the width of the distribution in Eq. (20) $2\langle\theta^2\rangle_\infty/\eta^2$ becomes smaller.

In the limit that η is small, the full width at half height of the distribution in Eq. (21) is $2\sqrt{\langle\theta^2\rangle_\infty 2\ln 2/\eta^2}$ and can be used to determine the sensitivity of the signal phase on η. For example, the full width at half height in Fig. 4c of 0.2° translates into a tip angle error of only $\eta = 0.08°$. The remarkable feature of the data in Figs. 3 and 4 is the insensitivity of t_{delay} to tip angle error. The comparison of t_{delay} with theory for $\eta = 0$ in Table 1 suggests that the actual $\eta = 0.08°$ error in the data sets in Fig. 4c does not appreciably affect t_{delay}. To appreciate this dependence on η consider the most probable value t_{delay} from the integral of $T_R \ln(2/\theta_-)$ over the θ_- weighted distribution function in Eq. (20). Since the distribution function in Eq. (20) depends on both η and ϕ_-, the resulting integral which extracts the most probable value of θ_- will also depend on η and ϕ_- as

$$t_{\text{delay}} = \frac{T_R}{2}\ln\left(\frac{4}{\theta_-^2}\right) \approx \frac{T_R}{2}\ln\left(\frac{4}{\langle\theta^2\rangle_\infty + \eta\cos\phi_-\sqrt{\langle\theta^2\rangle_\infty}}\right) \qquad (22)$$

where quadratic and higher-order terms in η are neglected. Notice that for $\eta^2 \ll \langle\theta^2\rangle_\infty$, Eq. (22) reduces to Eq. (15). This relation implies that unless $\eta^2 \gg \langle\theta^2\rangle_\infty$, t_{delay} will not appreciably change from the $\eta = 0$ value. Also, since the η dependence following integration over θ_- still remains in the natural logarithm the overall effect of η on t_{delay} will be less pronounced.

In summary, we have shown that a Gaussian–Boltzmann distribution in the tipping angle degree of freedom of a single vector magnetization M_0, governed by the circuit resistance temperature, accounts for the evolution in time of radiation damping emission of Zeeman energy from the inverted state, and also for the evolution toward equilibrium with the circuit near the ground state. Further refinement of the theory will take into account magnetic field inhomogeneity. The strong phase dependence of the hyperbolic secant radiation damping signal on tip angle error η may become a very sensitive detector of magnetic field. Any slight tip of the perfectly inverted magnetization from the $-z$ direction by either increased rf noise, low-level coherent rf, the bulk demagnetizing field of dilute solutes, or the radiation damping signal for a dilute solute, will induce the phase transition from random to coherent as in Fig. 3. It is this transition that could form the basis for an extremely sensitive measurement of NMR in dilute solution, much like the performance of an injection seeded laser in optical spectroscopy.

Acknowledgements

We thank Alex Pines for support and gratefully acknowledge the assistance of Thorsten Dieckmann in the course of data acquisition. M.P.A. thanks U.C. Davis and the Packard foundation for support during the course of this work.

References

[1] P. Bosiger, E. Brun, D. Meier, Phys. Rev. Lett. 38 (1977) 602.
[2] N. Bloembergen, R.V. Pound, Phys. Rev. 95 (1954) 8.
[3] R.H. Dicke, Phys. Rev. 93 (1954) 99.
[4] M.S. Feld, J.C. MacGillvary, in: M.S. Feld, V.S. Letokhov (Eds.), Coherent Nonlinear Optics, Springer, Berlin, 1980.
[5] M.P. Augustine, E.L. Hahn, J. Phys. Chem. 102 (1998) 8229.
[6] A. Sodickson, W.E. Maas, D.G. Cory, J. Mag. Res. B 110 (1991) 298.
[7] J.H. Chen, X.A. Mao, J. Phys. D 32 (1999) 764.
[8] T. Sleator, E.L. Hahn, C. Hilbert, J. Clarke, Phys. Rev. B 36 (1987) 1969.
[9] R. Glauber, F. Haake, Phys. Lett. 68A (1978) 29.
[10] Q.H.F. Vrehen, in: H. Walther, D.W. Rothe (Eds.), Laser Spectroscopy IV, Springer, Berlin, 1979.
[11] F. Haake, J.W. Haus, H. King, G. Schroder, R. Glauber, Phys. Rev. A 23 (1981) 1322.